npj | flexible electronics

Article

Published in partnership with Nanjing Tech University

https://doi.org/10.1038/s41528-026-00529-5

3D micropatterning of PEDOT:PSS/Gelatin conductive hydrogels *via* two-photon lithography for soft bioelectronics

Marco Buzio[1,2], Martina Gini[1,2], Tom C. Schneider[3], Nevena Stajkovic[1,2], Sven Ingebrandt[4], Laura De Laporte[3,5,6], Andreas Offenhäusser[2], Valeria Criscuolo[1,2] ✉ & Francesca Santoro[1,2]

The mechanical similarity between bioelectronic platforms and native tissue microenvironments is critical for successful cell-microdevice interfacing. Advances in high-resolution microfabrication have enabled the creation of 3D conductive microstructures; however, these approaches typically yield to structures that are electrically active but mechanically stiff relative to biological tissues. In this work, we present a strategy for the fabrication of soft 3D bioelectronic interfaces by blending PEDOT:PSS with a methacrylate-modified gelatin and leveraging two-photon polymerization lithography for micropatterning. Incorporating the conducting polymer into the hydrogel matrix resulted in reduced electrical impedance and exhibited soft mechanical properties both at the macro- and micro-scale. Here, the conductive hydrogel blends have been 3D printed, their versatility was assessed through different geometries and were used for neuronal cell culture. This approach enables the fabrication of soft neural interfaces with biomimetic architectures, using multimaterial blends, supporting improved electrical and mechanical integration at the cell-electrode interface.

The convergence of bioelectronics and living systems is advancing the design of human-machine interfaces toward enhanced adaptability and functional integration. Here, bio-hybrid interfaces play a pivotal role in facilitating direct communication between biological electrogenic tissues and electronic platforms. These systems might decode endogenous bioelectrical signals and could respond by generating precise electronic stimuli, thereby enabling real-time bidirectional interaction with for instance neuronal networks[1] and cardiac tissues[2]. However, biological systems are inherently soft[3,4], heterogeneous, and dynamic, requiring interface materials and architectures that not only minimize mechanical mismatch but also support bidirectional communication by converting ionic bioelectrical signals into electronic ones and vice versa. Here, a biomimetic design strategy is required, not only ensuring biocompatibility, but actively replicating the extracellular matrix (ECM) architecture that is fundamental for structural support and cell signaling[5,6]. This necessitates design principles such as mechanical recapitulation to match the elastic modulus and stress-relaxation behavior of native tissues[3], physicochemical fidelity to enable both ionic and electronic conductivity[7], and ultrastructural mimicry to reproduce the ECM's nano- to microscale architecture[8].

Biological tissues naturally exhibit complex 3D architectures with variable mechanical properties, surface features, and biochemical composition, which might tune cell behavior[9]. Previous works have exploited multiscale physical features, including microgrooves[10], micropillars[11] and scaffolds[12,13], to provide effective guidance cues that control cellular functions[14] and engineer cell-electrode interfaces[13,15], ultimately improving signal transmission[16–18] and enabling precise modulation of cellular behavior[13,14]. In this context, laser assisted printing techniques, such as two-photon polymerization lithography (TPL), facilitate the fabrication of multiscale 3D constructs *via* direct laser writing, enabling rapid prototyping of scaffolds and microelectrodes[19]. This technique utilizes a focused femtosecond laser to initiate polymerization upon the absorption of two photons within a specified volume (voxel) of a photocurable material (resist). The voxel is moved within the resist to realize the final construct. Typical materials used for this fabrication are acrylate- and methacrylate-based resins, which are yet biocompatible but rather stiff and non-conductive. To overcome this, one approach for creating conductive microstructures involves coating non-conductive resin printed through TPL with conductive materials like gold[20] or organic conductive polymers *via* chemical[21] or

[1]Neuroelectronic Interfaces, Faculty of Electrical Engineering and IT, RWTH Aachen University, Aachen, Germany. [2]Institute of Biological Information Processing IBI-3, Forschungszentrum Jülich, Jülich, Germany. [3]DWI-Leibniz Institute for Interactive Materials, Aachen, Germany. [4]Institute of Materials in Electrical Engineering 1, RWTH Aachen University, Aachen, Germany. [5]Institute of Technical and Macromolecular Chemistry (ITMC), Chair of Macromolecule Materials for Medicine, RWTH Aachen University, Aachen, Germany. [6]Institute for Applied Medical Engineering (AME), Department for Advanced Materials for Biomedicine, University Hospital RWTH Aachen, Aachen, Germany. ✉e-mail: v.criscuolo@fz-juelich.de

electrochemical[19,22] deposition. Another strategy is to focus on developing materials that are intrinsically conductive and compatible with the TPL process[23,24]. This includes incorporating electroactive fillers, such as carbon nanotubes[25], graphene-based materials[26], conjugated polymers[27–29], and various inorganic materials such as gold[30], silver[31], and other metals[32], into the photocurable resins.

Although these approaches and materials offer the required conductivity for microstructures, they are often stiff and not well-suited for applications involving soft biological tissues.

Here, conductive hydrogels (CHs) have emerged as key materials for the development of tissue-like and compliant electronic devices, serving as an effective bridge between rigid electronics and soft biological tissues[7,33]. CHs are realized by integrating conductive fillers, such as carbon nanotubes (CNTs), graphene derivatives, or inorganic materials, into a hydrophilic polymer network[34]. However, these systems can suffer from surface energy mismatch between the hydrophilic hydrogels matrix and the hydrophobic fillers, preventing an effective three-dimensional charge percolation, requiring complex, multistep processing to enable sufficient dispersion and loading[35]. Among the various conductive fillers, conjugated polymers (CPs) stand out thanks to their superior chemical tunability, mechanical flexibility, biocompatibility, and solution processability[35]. In addition, organic mixed ionic-electronic conductors (OMIECs), such as poly(3,4-ethylenedioxythiophene) polystyrene sulfonate (PEDOT:PSS), play a pivotal role in this context by being able to mediate ionic signal transduction across the biotic and abiotic domains[36].

Such materials are incorporated as electroactive components to engineer pristine or doped polymeric CHs that overcome the limitations of inorganic fillers, with numerous studies highlighting PEDOT: PSS as a particularly promising candidate[34,35,37].

Although PEDOT:PSS itself is not photocurable, it can be combined with photo-crosslinkable hydrogel matrices that allow photopatterning while retaining electroconductivity[28].

Here, synthetic and natural polymers like polyethylene glycol (PEG) and gelatin are well-known biomaterials whose methacrylate form can be employed to develop photocurable hydrogels[38]. Polyethylene glycol diacrylate (PEGDA) lacks inherent bioactive sites and requires functionalization with peptides or proteins to enhance cell interactions and biodegradation. On the other hand, gelatin, a denatured form of collagen containing bioactive motifs (*e.g.*, Arg-Gly-Asp, RGD sequences), represents an excellent biomaterial candidate for tissue engineering applications due to its biocompatibility and cell-supporting properties[39], however it lacks electrical conductivity and photopatterning capabilities. To overcome the latter, gelatin can be chemically modified by introducing methacrylate functional groups to the gelatin backbone, yielding gelatin methacryloyl (GelMA), that can undergo covalent crosslinking between protein chains under UV irradiation in the presence of a photoinitiator[40]. Interestingly, the chemical modification with methacrylate moieties preserves the biological characteristics of the original peptide sequence while introducing photo-crosslinking functionality. Indeed, GelMA-based resists have been extensively studied in the context of TPL, finding applications as soft scaffolds for cell adhesion[38,41]. Therefore, combining PEDOT:PSS with GelMA[42], can represent an effective approach to develop soft electronic platforms, with CHs that not only meet the mechanical and electrical requirements of cell-electrode interfacing but also provide a cell-friendly, degradable scaffold that better interfaces with living tissues. However, PEDOT:PSS/GelMA blends have been exploited so far as macroscopic scaffolds[42] and their application in TPL, which could allow for the production of soft bio-derived microelectrodes and interfaces with design flexibility at cell-level precision, remains underexplored.

In the present study, we developed PEDOT:PSS/GelMA-based photoresists with variable PEDOT:PSS concentrations able to be 3D photopatterned through TPL yielding sub-100 μm structures. First, the blends were mechanically and electrochemically characterized as bulk materials through one-photon UV crosslinking to assess the macroscopic properties. Then, we investigated the TPL conditions for each blend, by screening the delivered dose required to initiate photo-crosslink and by varying patterned geometries including square, round, sharp-edged and stylized neuron-like shapes. Printing fidelity was evaluated to compare the design with the resulting microstructure. This dual focus on processing conditions and structural fidelity provides insight into the functional flexibility of these new photoresist formulations for high-resolution 3D soft microfabrication. Additionally, mechanical and electrochemical analyses were carried out on the 3D microstructures to verify that such features were preserved at the microscale. As proof of concept, transparent multielectrode arrays (MEAs), featuring indium tin oxide (ITO) electrodes and feedlines, were coated with the 3D printed CHs to evaluate their potential as microelectrodes for in vitro devices. Finally, the biocompatibility of the patterned microstructures was evaluated with in vitro neuronal cell models. The proposed strategy can advance the development of soft bioinspired electronics, able to recapitulate the native environment of biological systems for close interfacing, finding applications as biosensors and recording/stimulating electrodes.

Results

Development and characterization of photopatternable CHs

To impart electrical conductivity to the photopatternable GelMA, PEDOT:PSS was blended at different ratios, yielding three formulations containing 0.0% w/v, 0.3% w/v, 0.5% w/v of PEDOT:PSS in a 10% w/v GelMA in Milli-Q water, namely GP0, GP3 and GP5, respectively (Fig. 1a, Methods section). For all formulations, 3% w/v of the water-soluble lithium phenyl-2,4,6-trimethylbenzoylphosphinate (LAP) was added, providing a Norrish Type I photoinitiation systems.

First, GelMA was prepared as described in the Methods section and in Fig. S1a. Here, the degree of modification (DoM) was calculated as the ratio between integral of the free amine ^{1}H-NMR signal of synthetized GelMA and pristine gelatin and it was used to quantify the amount of covalently bonded methacrylate moieties (Fig. S1b)[39].

In this work, all experimental studies were conducted using GelMA with a standardized DoM of ~ 70%.

The photogelation process of the resulting blends was monitored by measuring the variations in the storage modulus (G') as a function of time through photoreology (Fig. 1b, Methods section). After an initial conditioning phase of 60 s, G' increased upon UV irradiation over time, finally reaching a plateau value of ~ 2 kPa suggesting successful photopolymerization for all material formulations. Here, the plateau region, reached following UV irradiation, revealed minimal variation in G' values among the different PEDOT:PSS concentrations whereas a modest increase in the loss modulus (G") was observed. (Figure S2). All PEDOT:PSS-based blends exhibited photo-crosslinking kinetics like pristine GelMA, while displaying higher initial G' values: this increase in G" can be attributed to enhanced intermolecular interactions between the negatively charged sulfonic acid groups of PSS and the positively charged amino acid residues (*i.e.*, arginine and lysine) within the gelatin backbone[43].

Then, to evaluate the microstructure of the resulting blends, scanning electron microscopy (SEM) imaging of bulk samples showed an influence of PEDOT:PSS content on the porous microstructure and overall network organization of the hydrogels (Fig. 1c). In particular, blends with a higher PEDOT:PSS concentration (*e.g.*, GP5) exhibited a more compact and uniform network with a microstructural arrangement more densely interconnected, as compared to formulations containing less PEDOT:PSS. Conversely, GP3 presented a network with larger, more irregularly distributed pores and a less cohesive structural arrangement. This result indicates that the incorporation of PEDOT:PSS acts as an effective modulator of the hydrogel's internal architecture that can affect key properties of printed hydrogel constructs[44].

In order to investigate the conductivity of the synthesized blends, electrochemical impedance spectroscopy (EIS) was employed to characterize the bulk electrical properties of swollen hydrogels. Here, crosslinked cylinders of 10 mm diameter and 1 mm thick, were placed between two gold electrodes (Methods section). The impedance spectra (Fig. 1d) showed that all formulations exhibited characteristic frequency-dependent behavior, with PEDOT:PSS-based hydrogels displaying reduced impedance at 1 kHz

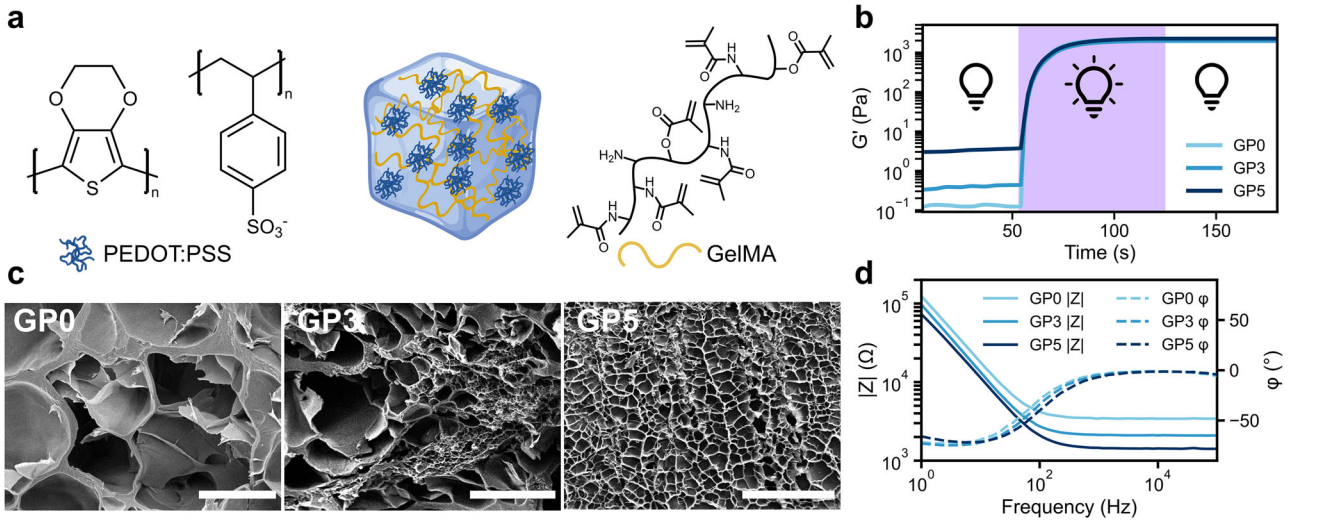

Fig. 1 | Design and characterization of PEDOT:PSS/GelMA blends and bulk structures. a Schematic illustration of the molecular design and photo-crosslinked GelMA/PEDOT:PSS CH. **b** Representative photorheology curves showing the evolution of the storage modulus (G') over time for CHs containing different PEDOT:PSS contents ($N = 4$). The shaded purple region indicates the UV exposure period during photopolymerization. **c** Scanning electron micrographs of cross-sectional morphologies of bulk UV-photo-crosslinked GP0, GP3, and GP5 samples, highlighting microstructural differences induced by varying PEDOT:PSS concentrations (scale bars 20 μm). **d** Representative EIS Bode plots displaying the impedance modulus (| Z |) and phase angle (φ) for bulk photo-crosslinked GP0, GP3 and GP5 hydrogels measured between two gold electrodes ($N = 3$).

relative to the pristine counterpart, which decreased from 3.1 ± 0.9 kΩ for GP0 to 1.6 ± 0.2 kΩ for GP5 formulations ($p < 0.05$, $N = 3$). Here, the electrostatic interactions between PEDOT:PSS and gelatin may disrupt the π-π stacking and conjugated backbone alignment of PEDOT chains[36]. In addition, the formation of ionic complexes between PSS and gelatin amino groups can reduce the doping availability of PSS[45], therefore requiring a higher PEDOT:PSS concentration in the blends[35]. Nevertheless, these results demonstrated that PEDOT:PSS incorporation successfully enhances the electrical conductivity of GelMA even at low concentration.

Two-photon polymerization patterning and characterization

To evaluate the suitability of the developed blends as photoresist materials for two-photon polymerization (2PP), their photo-crosslinking response upon two-photon irradiation was investigated under varying laser powers, assessing if PEDOT:PSS concentration affects the materials.

First, the laser power required to initiate polymerization, namely the polymerization threshold, was determined for each blend across a range of PEDOT:PSS concentrations (Fig. S3). Here, structures were printed in oil configuration, in which the laser goes through the glass substrate to reach the photoresist, keeping the gelatin-based blends in solid state during the printing process therefore impeding objective immersion in the resist. The polymerization threshold decreased with increasing PEDOT:PSS concentration, from 7 mW for GP0 to 2 mW for GP5. A similar trend was observed for the damage threshold, defined as the laser power at which visible physical degradation occurs, such as bubble formation during laser exposure, that decreased from 28 mW for GP0 to 23 mW for GP5. On the other hand, the intermediate blend (GP3) exhibited a slight increased damage threshold to 30 mW (Fig. S3). These observations suggest that increasing PEDOT:PSS content in CH blends can facilitate polymerization at lower laser powers, but also reduces the damage threshold, with the exception of GP3. In fact, it has been reported that PEDOT:PSS can enhance the rate of photopolymerization in hydrogel systems[7], due to the presence of PSS chains that can facilitate free-radical generation, either by improving the efficiency of the photoinitiator system or by participating in electron transfer reactions characteristic of Norrish Type II mechanisms[46]. In such systems, the polyanionic nature and redox activity of PEDOT:PSS promote electron transfer between the excited photoinitiator and a co-initiator, thereby increasing radical production[43,46]. Although this mechanism does not apply in Norrish Type I photoinitiation systems, that proceed *via* unimolecular bond cleavage, it can be hypothesized that the reduction of the polymerization and damage threshold for GP5 could be attributed to the presence of the sulfonic acid groups on PSS, that may interact with the photoinitiator or stabilize free radicals, potentially altering the polymerization process and enabling faster monomer conversion under light exposure.

In addition, the capability of the resists to realize diverse geometries was explored, creating both curved geometries, such as cylindrical shapes, and sharp-edged patterns, exemplified by star-like designs.

Hydrogel-based materials have the intrinsic ability to absorb and retain significant amounts of water, leading to swelling for which the hydrogel undergoes volumetric expansion upon hydration. As a result, the final dimensions of the hydrogel microstructures may deviate from their original specifications as defined in the CAD model. Based on the previous results, the fabrication window, the range of laser powers between polymerization and damage thresholds[47], and possible swelling of GP0 and GP5 were investigated by analyzing the congruence of the resulting shape of printed cylinders with the designed CAD (Fig. 2a-i, ii, respectively). Initially, it was observed that GP5 cylindrical structures could be polymerized with a laser power as low as 5 mW, whereas GP0 required a minimum of 20 mW. However, for GP5, a laser power above 20 mW led to overexposed structures. Therefore, two distinct laser power ranges were used to fabricate cylindrical structures while keeping the scan speed consistent for both blends, ranging from 3 mm s^{-1} to 9 mm s^{-1} in 2 mm s^{-1} steps. Due to the different laser power ranges, the total delivered dose (*i. e.* the combination of laser power and scan speed) to the structures varied for GP0 and GP5, therefore, only structures exposed with comparable dose values were included in the analysis. Figure 2a-iii shows that deviations in cylinder radius from the original CAD model were found to be comparable across structures fabricated with similar exposure doses, regardless of the PEDOT:PSS concentration.

To verify the three-dimensionality of the printed structures, cylinders fabricated from GP0 (20 mW, 3 mm s^{-1}) and GP5 (5 mW, 5 mm s^{-1}) were imaged using a confocal microscope and Z-stacks were acquired (Fig. S4). The analysis revealed average structure height of 28.64 μm ± 4.80 μm for GP5 and 29.81 μm ± 1.91 μm for GP0, which are in close agreement with the nominal CAD model height of 30 μm, confirming accurate vertical reproduction of the printed features.

Following this analysis, the fabrication window of GP3 and GP5 for cubical structures was investigated by printing arrays of cubes (30 μm × 30 μm × 30 μm) varying the laser power (from 5 mW to 20 mW,

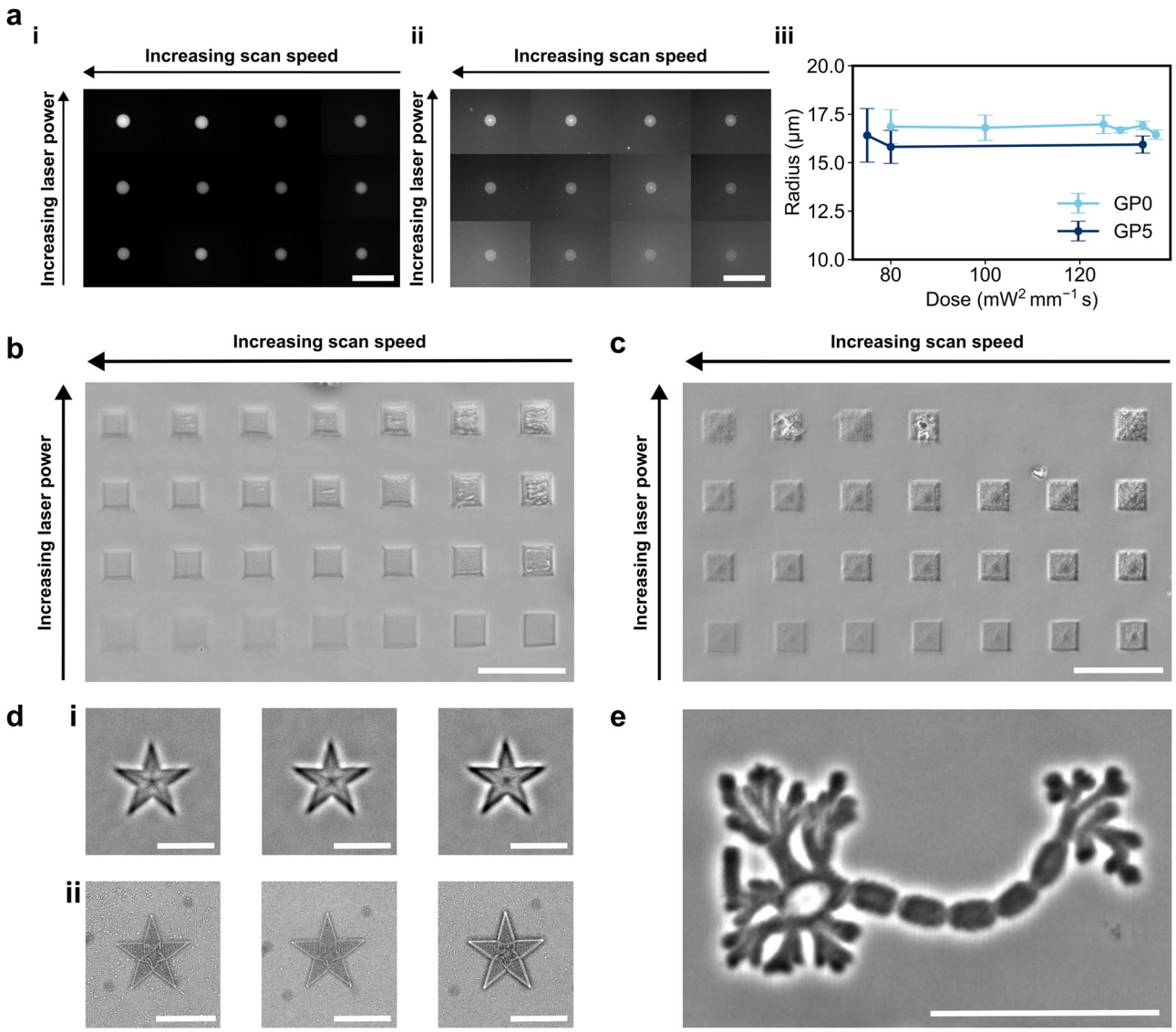

Fig. 2 | Characterization of 2PP micropatterning of PEDOT:PSS/GelMA blends. **a** Shape analysis of 2PP fabricated cylindrical microstructures composed of **i** GP0 and **ii** GP5 formulations, alongside **iii** quantification of the average outline radius from three independent measurements obtained from the analysis of fluorescence microscopy images of post-fabrication stained structures (scale bars 100 µm). **b, c** Bright field microscopy images of 2PP dose tests of **b** GP3 and **c** GP5 formulations photopatterned as parallelepipeds, illustrating the effect of increasing scan speed and laser power and composition on structure formation (scale bars 100 µm). **d** Bright field images of 2PP fabricated star-shaped microstructures based on **i** GP3 and **ii** GP5 compositions, with progressively higher writing doses from left to right (scale bars 30 µm). **e** Bright field image of a GP5-based neuron-inspired microstructure fabricated *via* 2PP (scale bar 50 µm).

intervals 5 mW) and scan speed (from 3 mm s^{-1} to 15 mm s^{-1}, intervals of 2 mm s^{-1}) (Fig. 2b, c, respectively). The investigated exposure window was applied to both CHs, with GP5 exhibiting sharper feature edges at lower doses compared to GP3. This allowed the selection of 5 mW laser power and 5 mm s^{-1} scan speed as benchmark parameters for subsequent experiments. Therefore, stars, with 30 µm circumscribed circle radius and 10 µm thick (Fig. 2d), and stylized neuron-like structures, of maximum length 100 µm and 10 µm thick (Fig. 2e), were printed thus demonstrating the possibility to realize defined structures with different features. In addition, confocal Z-stack acquisitions were performed to confirm the congruence of the printed stylized neuron-like structures with the CAD model even for such complex shapes (Fig. S5). In particular, the measured thickness for GP0 was found to be 14.94 µm ± 5.66 µm, thus deviating from the design, and 9.71 µm ± 1.96 µm for GP5, suggesting that the presence of PEDOT:PSS can reduce swelling effects of the blends as compared to the pristine GP0[44].

Afterwards, the mechanical properties of 3D microstructures were investigated through nanoindentation on cubical structures (Fig. 3a). The analysis revealed that increasing PEDOT:PSS content did not induce relevant variations in the Young's modulus across the tested formulations; the measured values remained consistently low, in the range of ~ 1 kPa, highlighting the soft mechanical properties of the hydrogels, closely mimicking brain tissues[48]. The Young's modulus measured 1.09 kPa ± 0.19 kPa for GP0, 1.05 kPa ± 0.58 kPa and 0.83 kPa ± 0.25 kPa for GP3 and GP5, respectively. The low impact on the modulus likely reflects the ability of water-rich networks to integrate conductive components without compromising the inherent compliance of the hydrogel[49].

Additionally, parallelepipeds were printed on a glass substrate and probed with two tungsten needles in order to characterize the conductivity of the blends at the microscale. The current-voltage (I-V) scans confirmed that incorporating PEDOT:PSS into the pristine GelMA matrix led to increased electrical conductivity, even at the microscale. In particular, the GelMA alone exhibited a conductivity of approximately 0.5 ± 0.02 mS cm^{-1}, while the PEDOT:PSS-containing blends showed higher values: GP3 reached about 0.8 ± 0.02 mS cm^{-1} and GP5 improved to approximately 0.9 ± 0.07 mS cm^{-1} (Fig. S46). The measured conductivities are in accordance with previously reported values of hydrogel-based blends, that

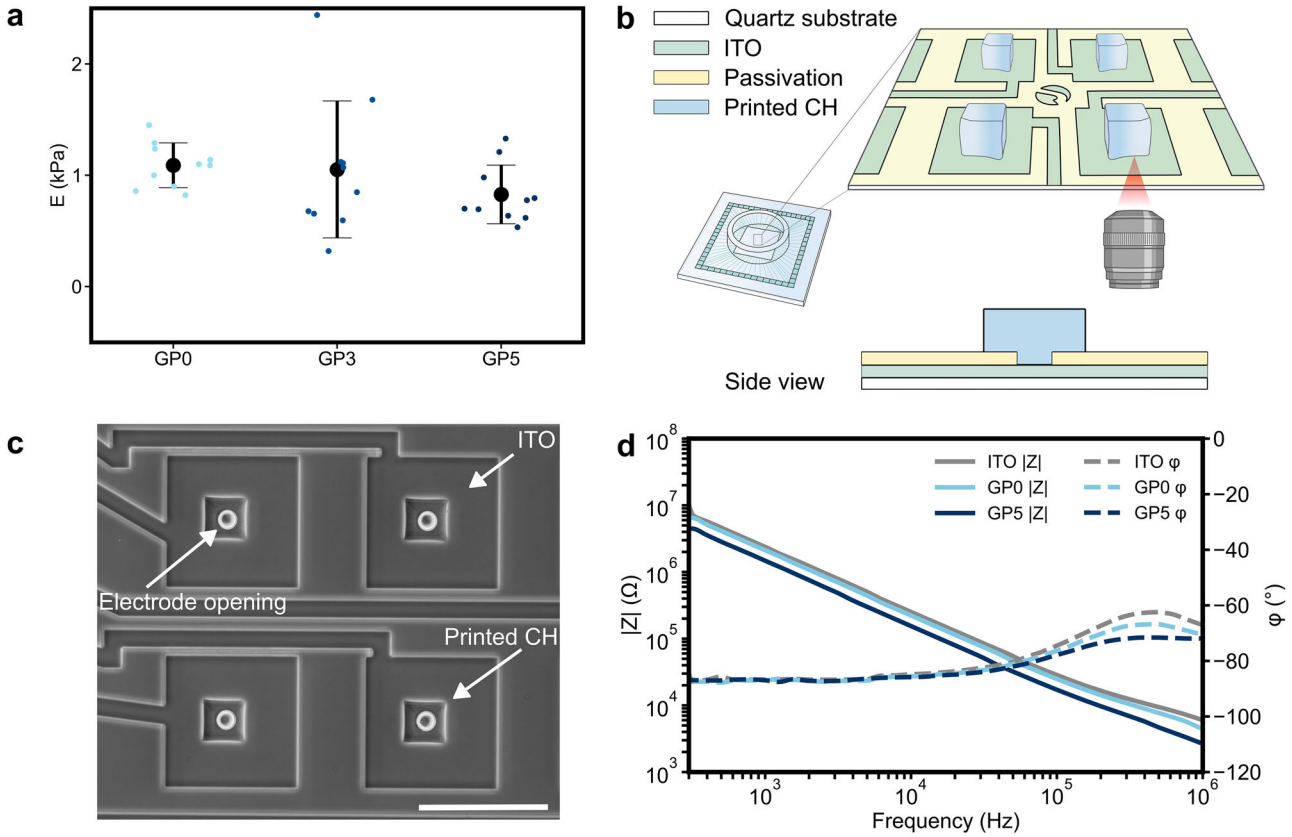

Fig. 3 | Mechanical and electrochemical characterization of 2PP printed PEDOT:PSS/GelMA microstructures. a Young's Modulus (*E*) calculated from nanoindentation measurements in Milli-Q water of CHs printed *via* TPL ($N = 10$). **b** Schematic representation of the 3D transparent soft MEA, shown in tilted and side views (illustrations not in scale). **c** Bright field microscopy image of 2PP printed CH structures photopatterned on a transparent MEA, imaged from the bottom of the substrate (scale bar 200 µm). **d** Representative EIS Bode plots showing impedance modulus (| Z |) and phase angle (φ) responses of bare ITO electrodes (grey trace) and electrodes coated with patterned GP0 (light blue trace) and GP5 (dark blue trace) blends, measured in DPBS ($n = 3$, $N = 3$).

incorporate metals, CNT and graphene as conductive fillers employed in bioelectronics[7], and meet the requirements for brain tissue engineering[48].

To evaluate the relevance for bioelectronic applications, complementary EIS measurements were performed in Dulbecco's phosphate buffered saline (DPBS) to simulate tissue-like ionic environments and to assess the electrochemical properties of GP0 and GP5, printed as cubical structures, onto transparent ITO-based MEAs (Fig. 3b, c). Here, the transparent electrodes were instrumental to allow the oil printing modality, employing a long working distance objective (20× air) to focus the laser through the thick quartz substrate. The results revealed that the 3D CH-based microstructures led to a lowered impedance, especially in the presence of PEDOT:PSS. The average impedance of electrodes coated with GP5 exhibited a considerable reduction of approximately 30% compared to the baseline planar, uncoated electrodes, calculated at 1 kHz (Fig. 3d). This decrease in impedance is indicative of enhanced charge transfer capabilities and improved electrical interfacing[1]. In contrast, electrodes coated with GP0 showed a much smaller reduction in impedance, averaging only about 7% relative to the uncoated control. This slight improvement suggests that GelMA alone provides limited benefits in terms of electrical conductivity, likely due to its primarily ionic, rather than electronic, conduction properties. The observed reduction in impedance can be attributed to two primary factors. First, 3D microstructures increase the effective surface area of the electrode, thereby enhancing charge transfer across the interface. Second, the intrinsic conductive properties of PEDOT:PSS further lower the impedance by providing a more efficient pathway for electronic charge transport.

Cell interfacing

To assess the biocompatibility of microstructured blends, stylized neuronal patterns were printed on standard glass coverslips using TPL. First, the stability of the patterns was evaluated by soaking the samples in DPBS at 37 °C, over a period of 14 days, and monitoring *via* optical microscopy possible detachment from the substrate and/or shape distortions. Results revealed that all the blends remained stably attached to the glass coverslip up to 4 days, while GP0 showed pronounced swelling leading to structure distortion at day 4 and complete detachment at day 8 (Fig. S7). These results suggest that the presence of PEDOT:PSS can stabilize the 2PP patterned blends both in terms of adhesion and shape retention over time in physiological conditions[44].

Afterwards, two types of cell models were employed to perform the biocompatibility assessment: primary rat cortical neurons (pRCN) and neuronal HT22 cells, a well-characterized immortalized mouse hippocampal cell line. Cells were cultured on top of the patterned substrates (Fig. S8) and the viability was evaluated at four days in vitro (DIV 4). Cell viability was quantified through live/dead assay, labeling live cells with the green fluorescent dye Calcein AM (λ_{ex} 496 nm, λ_{em} 516 nm), and dead cells with the red fluorescent dye ethidium homodimer (λ_{ex} 528 nm, λ_{em} 617 nm), allowing to calculate the ratio between live cells and the total cell number as the sum of live and dead cells (Methods section, Fig. 4a, Fig. S9 and Fig. S10). Culturing primary cortical neurons and HT22 hippocampal cells with the microstructured blends did not significantly impair overall cell viability, as confirmed by live/dead assay results (Fig. 4b and Fig. S9b, respectively), revealing survival rates consistent with those observed under control conditions (PLL-coated glass) and indicating that the CH structures do not induce any cytotoxic effect. Specifically, the control condition showed a live/dead ratio of 46.11% ± 8.78%, whereas GP0, GP3, and GP5 exhibited ratios of 54.19% ± 7.45%, 49.23% ± 8.65%, and 52.5% ± 6.7%, respectively. Moreover, HT22 showed a live/dead ratio of 99.22% ± 2.28% on control substrates, and ratios of 99.94% ± 0.17%, 98.57% ± 2.56% and

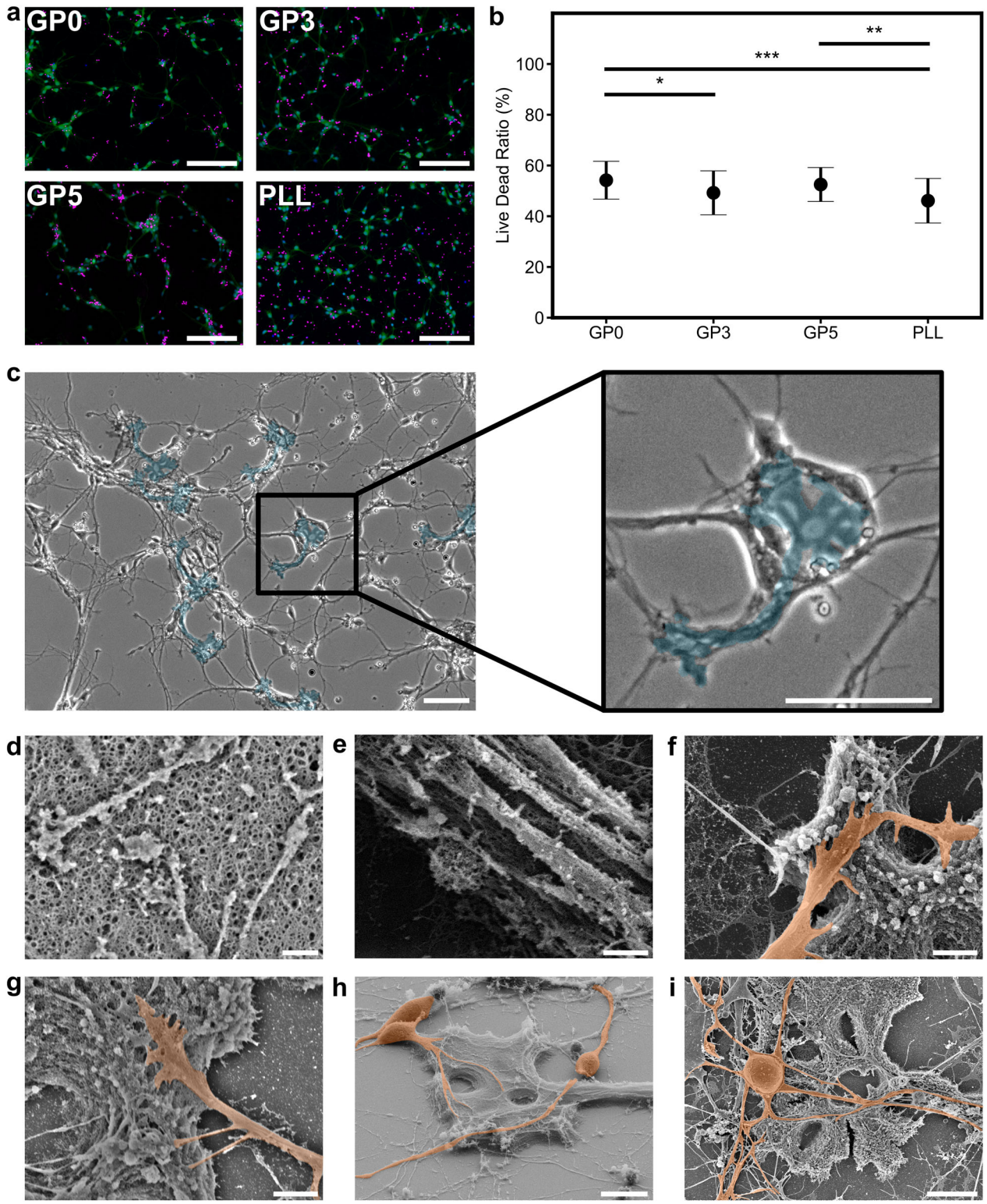

Fig. 4 | Biocompatibility assessment and neuronal cell interfacing on 2PP printed PEDOT:PSS/GelMA microstructures. a pRCN cultures grown for four days in vitro on poly-L-lysine (PLL) coated, 2PP patterned GP0, GP3 and GP5 substrates, as well as on PLL coated glass coverslips, labeled with fluorescent markers for cell nuclei (blue), live cells (green), and dead cells (magenta) (scale bars 150 µm). **b** Quantitative analysis of pRCN viability, expressed as live/dead cell ratio reported as mean ± standard deviation (***$p < 0.0001$, **$p < 0.01$, *$p < 0.05$, $n = 3$, $N = 3$). **c** Bright field microscopy image showing neuronal growth on a GP5-based 2PP patterned substrate at DIV4; printed microstructures are pseudo-colored in light blue for visualization (scale bars 50 µm). **d, e** Scanning electron micrographs displaying the nanofibrous morphology of 2PP printed GP5 hydrogel networks at different magnifications (**d** scale bar 400 nm, **e** scale bar 1 µm). **f, g** Scanning electron micrographs illustrating pRCN membrane processes (pseudo-colored in orange) extending over 2PP printed stylized neuron-shaped microstructures (**f, g** scale bars 2 µm). Scanning electron micrographs showing pRCN attachment and spreading (false colored in orange) on 2PP printed **h** GP5 and **i** GP0 (scale bars 10 µm).

99.16% ± 3.11% for GP0, GP3 and GP5, respectively. In addition, since nano- and micro-topographies can influence cell behavior, adhesion and processes outgrowth[8], we investigated cellular adhesion and interaction with the 3D patterned blends. Bright field microscopy imaging suggested an interaction between primary neurons and the printed stylized neuronal patterns (Fig. 4c). SEM imaging revealed that the nanofibrous network present on the patterned CH surfaces (Fig. 4d, e) closely mimics the architecture of the native ECM. Scanning electron micrographs showed that primary neurons interfacing with the CH structures exhibited an intimate attachment to the nanofibrous substrate (Fig. 4f–i).

Discussion

This work presents an innovative strategy to realize microstructured CHs for soft bioelectronics. By blending PEDOT:PSS with the modified photopatternable GelMA, we realized CH-based photoresists with soft mechanical properties of ~ 2 kPa of storage modulus following UV irradiation at the macroscale. EIS revealed that CHs displayed reduced impedance values as compared to the pristine GelMA. The 2PP processability of the blends was systematically investigated defining the printing window in terms of delivered dose, as a combination of laser power and scan speed, revealing distinct printing conditions according to the presence and concentration of PEDOT:PSS that facilitates lower doses needed for photo-crosslinking. Moreover, we demonstrated high printing flexibility and versatility by creating patterns with different geometries from smooth to sharp edged structures, exemplified by cylinders, cubes and stars, as well as biomimetic neuron-like geometries. Nanoindentation confirmed the soft nature of the 3D microstructures, with Young´s modulus value of ~ 1 kPa, while I-V scans confirmed the effect of PEDOT:PSS in increasing the electrical conductivity of the CH with respect to GelMA. The incorporation of PEDOT:PSS in the hydrogel network not only improved conductivity but enabled the fabrication of soft electrodes combining high electronic performance with tissue-like mechanics. Additionally, the 3D soft CH microstructures were fabricated onto the electrode openings of a transparent ITO-based MEA, lowering the overall electrodes' impedance. The increased effective electrodes´ surface could potentially enhance the coupling with biological tissue and cells providing a mechanically and electrically compliant interface. The successful implementation of this transparent 3D soft microstructured MEA serves as a critical proof-of-concept, demonstrating the feasibility of our fabrication approach that could be translated to flexible and transparent substrates. Finally, cell viability was proved on both immortalized and primary neurons, where the incorporation of PEDOT:PSS did not hamper cell viability. Scanning electron micrographs suggested that the 3D micropatterned CHs can facilitate an intimate contact between the cells and the biomimicking scaffold. The preliminary biological validation in this study, limited to short-term culture (4 days) and assessment of viability and morphology, paves the way towards further functional assays, such as neurite outgrowth quantification and electrophysiological recordings, to corroborate the material's role in improving electrical and mechanical integration. The combination of structural tunability, mechanical compliance, and electrical conductivity positions the developed CHs as promising candidate materials for future development of implantable neural devices and advanced culture systems that mimic the native neural microenvironment as next-generation bioelectronic devices.

Methods

Synthesis and characterization of GelMA

Gelatin methacrylolyl (GelMA) was synthetized as previously reported[40]. Gelatin from bovine skin (10 g, gel strength ~225 g Bloom, Type B, Sigma-Aldrich Chemie GmbH, Germany) was dissolved in DPBS (100 mL, Thermo Fisher Scientific Inc., Germany) at 45 °C under slow stirring. Then, methacrylic anhydride (6 mg, Sigma-Aldrich Chemie GmbH, Germany) was added drop wise to gelatin solution at 0.6 mg per gram of gelatin, and the solution was heated at 50 °C while stirring vigorously. After 3 h, warm DPBS (200 mL, 45 °C) was added to the solution to stop the reaction. The solution was then centrifugated at 3500 *g* for 4 min at RT, resulting in the deposition of a white pellet. The clear supernatant was collected and transferred to a dialysis tube (MWCO 12400 Mw, Sigma-Aldrich Chemie GmbH, Germany) and dialyzed against Milli-Q water at 40 °C for 4 days changing dialysis medium twice a day. Finally, the solution was freeze-dried for two days. The resulting foam was stored at -20 °C up to three months.

The degree of modification (DoM) was assessed *via* proton nuclear magnetic resonance (^{1}H-NMR) performed with an Avance III 600 MHz (Bruker, USA) spectrometer, operating at 600.0 MHz (^{1}H). The samples (100 mg mL^{-1}) were dissolved in D_2O (Sigma-Aldrich Chemie GmbH, Germany) at 45 °C for 30 min. Chemical shifts refer to the residual water peak (H_2O, δ = 4.7 ppm for ^{1}H-NMR). Typical acquisition parameters for ^{1}H spectra were: 45 °C, 10 s of recycle delay, 12 scans, and the excitation sculpting water suppression was applied to the pulse program. The phenylalanine signal between 6.9 ppm and 7.6 ppm was taken as reference and used to normalize all the spectra, since this peak is proportional to polymer concentration[50]. The amount of lysine methylene signal (between 3.0 ppm and 3.25 ppm) has been considered to quantify the number of free -NH_2 moieties still present after the reaction with methacrylic anhydride[50]. These signals were integrated in both gelatin and GelMA spectra to obtain their area and the DoM of GelMA samples was calculated following Eq. (1):

$$DoM = \left(1 - \frac{Lysine\ protons\ of\ GelMA}{Lysine\ protons\ of\ gelatin}\right) * 100 \quad (1)$$

Preparation of GelMA/PEDOT:PSS blends

Three photoresist formulations were prepared using GelMA as the base material: two conductive variants (GP3, and GP5) and one non-conductive control (GP0). The conductive photoresists were created by incorporating PEDOT:PSS (Clevios PH1000, Heraeus Deutschland GmbH & Co. KG, Germany) at varying concentrations of 0.3% w/v (GP3), and 0.5% w/v (GP5), while the control formulation (GP0) contained no PEDOT:PSS. All formulations maintained consistent concentrations of 10% w/v GelMA and 3% w/v LAP (Sigma-Aldrich Chemie GmbH, Germany) in Milli-Q water.

PEDOT:PSS dispersion was sonicated at 4 °C for 30 min and filtered with 0.22 µm polytetrafluoroethylene (PTFE) syringe filter (TH. Geyer, Germany). Filtered solution was allowed to warm up to RT before dropwise blending with GelMA under vigorous stirring at 50 °C. During preparation, the mixture was maintained in the dark to avoid exposure to light preventing crosslinking. After preparation, the solution was stored in a 4 mL amber vial at 5 °C for up to two weeks.

Photoreology

Photopolymerization kinetics of hydrogels were investigated through photorheology employing a Discovery Hybrid Rheometer HR20 (TA instruments, Germany), equipped with a UV curing module in conical-plate mode (20 mm diameter, 0.2 mm gap) at room temperature. Photorheological measurements were performed at 1 Hz oscillatory frequency and with 1% strain amplitude. The light source (365 nm, 5 mW cm^{-2}) was activated 60 s after initiating the measurement to stabilize the system before beginning the photopolymerization process and was then deactivated after 60 s. The evolution of the storage (G') and loss (G") modulus during the time was recorded to evaluate the polymerization kinetics.

Electrochemical characterization of bulk hydrogels

For electrochemical experiments, cylindrical hydrogels were fabricated. The photoresist was heated at 50 °C into a water bath for 10 min until the mixture was liquid. The solution (80 µL) was cast into a circular mold (inner diameter 10 mm, thickness 1 mm) and exposed to UV light (365 nm, 1 mJ cm^{-2}, E-Serie UV-Lamp, Spectroline®, Germany). After 15 min, the hydrogels were removed from the mold and developed in Milli-Q water for 1 h at 45 °C. The cylindrical samples were sandwiched between two gold coated glasses separated by a 0.9 mm spacer. Impedance spectroscopy data were recorded using a potentiostat/galvanostat (VSP-300, Biologic, Germany) interfaced with a desktop computer, equipped

with the EC-Lab software used to acquire signals. The sinusoidal input signal was set to 10 mV by scanning a range of frequencies from 1 Hz to 100 kHz. One-way ANOVA test, followed by a Tukey's multiple comparisons test, was performed to assess the statistical relevance of the impedance change according to the PEDOT:PSS content ($N = 3$).

Scanning electron microscopy of bulk hydrogels

Cylindrical hydrogels were prepared as explained above. The samples were subsequently immersed in liquid nitrogen for 10 min and freeze-dried. To obtain cross-sectional micrographs, the freeze-dried hydrogels were bisected with a sharp blade, mounted on stubs using double-sided carbon tape and sputter-coated with a thin layer of iridium (2 cycles, 15 mA, 60 s, thickness: ~ 7 nm, Emitech).

Substrate treatment

Glass coverslips and substrates were cleaned through a series of immersions and sonication in different solvents, each lasting 10 min. The process began with immersion in an Alconox (Sigma-Aldrich Chemie GmbH, Germany) solution in deionized water (10 g L^{-1}), followed by Milli-Q water, acetone (Sigma-Aldrich Chemie GmbH, Germany), and finally isopropyl alcohol (IPA, TH. Geyer, Germany). During each immersion, the coverslips were sonicated at high power. Finally, the substrates were dried using a nitrogen gun. To improve the adhesion of hydrogels to the glass substrates, the surface was functionalized with the silanization agent (3-(trimethoxysilyl) propyl) methacrylate (TMSPMA, Sigma-Aldrich Chemie GmbH, Germany) according to the manufacturer. After cleaning, the surface was activated with oxygen plasma (2 min, 100 W, O_2 flow 25 L min^{-1}, 0,8 mBar). Then substrates were submerged into a solution of abs. ethanol (50 mL, TH. Geyer, Germany), TMSPMA (0.25 mL) and diluted acetic acid (1:10 in Milli-Q water, 1.5 mL, Sigma-Aldrich Chemie GmbH, Germany). After 15 min, the substrates were rinsed with IPA and dried with a nitrogen gun. The silanized substrates were stored in the dark at RT for up to 1 week.

TPL patterning

Three-dimensional microstructures were printed *via* two-photon polymerization using a commercial system (Nanoscribe Photonic Professional GT Plus, Nanoscribe GmbH, Germany) operated in oil immersion mode (unless otherwise stated). The system employs a 780 nm Ti:sapphire laser delivering ~100 fs pulses at a repetition rate of 80 MHz, with a maximum power output of 150 mW. Structures were designed with CAD software and exported as stereolithography (STL) files. The STL files were converted into general writing language (GWL) scripts with DeScribe (Nanoscribe GmbH, Germany) software. The GWL scripts were designed in order to write the structures from top (furthest from the substrate) to bottom, minimizing optical aberrations caused by the polymerized gelatin, keeping the resist in solid state during fabrication[38]. Prior to printing, the photoresist was heated at 50 °C for 10 min, sonicated, and then dispensed (20 µL – 80 µL) onto a substrate pre-coated with the adhesion promoter TMSPMA. A rubber mold was placed on top to minimize evaporation. The resist was then stored at 4 °C for 45–60 min until it solidified. For fabrication, the substrate was mounted in a custom holder compatible with the piezoelectric x/y/z stage. Laser scanning trajectories were defined *via* a galvo-controlled x/y scanner. All the printings were performed at room temperature. Following exposure, the samples were developed in deionized water at 50 °C for 45 min. The structures were maintained in an aqueous environment throughout development and analysis to prevent irreversible collapse of the hydrogel network caused by drying.

Printability and shape analysis

To systematically compare the two-photon polymerization of the blends, both the polymerization threshold and the damage threshold were characterized. For these measurements, straight lines were printed on the XY plane while maintaining a constant scan speed of 100 µm s^{-1}. The laser power was increased from 1 mW up to 50 mW to determine the respective threshold values.

The radius of a series of cylindrical structures printed with different combinations of laser powers and scan speeds was measured to evaluate printing fidelity. Cylinders measuring 30 µm in diameter and 30 µm in height were printed using a 25× oil-immersion objective on silanized glass coverslips (thickness: 0.13 mm–0.16 mm, diameter: 13 mm). The structures were printed with a slicing distance of 1 µm and a hatching distance of 0.5 µm. Printing parameters were adjusted according to the formulation: for GP0, a laser power from 20 mW to 35 mW and a scan speed from 3 mm s^{-1} to 9 mm s^{-1} were applied; for GP3 and GP5, laser power was varied from 5 mW to 20 mW.

Fluorescent labeling was performed by adding 1 µL of a 1 mg mL^{-1} fluorescein isothiocyanate (FITC, Thermo Fisher Scientific Inc., Germany) solution in dimethylformamide (DMF, Sigma-Aldrich Chemie GmbH, Germany) to 1 mL of DPBS containing the printed samples. The samples were incubated for 2 h at room temperature in the dark to facilitate FITC conjugation. Following incubation, the structures were washed ten times with fresh DPBS to remove excess unbound dye, with each wash involving a 5 min incubation. Labeled structures were imaged using an epifluorescence microscope (Revolution, Discover Echo, USA) equipped with a 40× air objective. Structural outlines were manually segmented using Fiji (ImageJ), and shape accuracy was quantified by measuring perimeter, area, circularity, and ellipse fitting parameters ($N = 3$).

Confocal Z-stack acquisitions were performed using a laser scanning confocal fluorescence microscope (TCS SP8, Leica, Germany) equipped with a 20× oil objective. IMARIS software (Oxford Instruments, UK) was used to reconstruct the Z-stack and to generate the 3D images of the dataset. The height of each structure was calculated using Fiji (ImageJ), by measuring the mean fluorescence intensity of a region of interest (ROI) defined on the structure across all slices of the stack. Slices where the intensity exceeded 50% of the normalized maximum were identified, and the height was determined as the distance between the first and last slices meeting this criterion (cylinders: $n = 10$, $N = 3$; stylized neurons: $N = 3$).

Mechanical measurements of 2PP printed microstructures

Nanoindentation was carried out in Milli-Q water on cubic structures measuring 30 µm × 30 µm × 30 µm, printed on silanized glass coverslips (thickness: 0.13 mm–0.16 mm, diameter: 30 mm) with a 25× objective. The structures were printed with a slicing distance of 1 µm and a hatching distance of 0.5 µm. Printing parameters varied by formulation: for GP0, a laser power of 20 mW and scan speed of 3 mm s^{-1} were used; for GP3 and for GP5 5 mW and 5 mm s^{-1}. The glass slides comprising the printed cubic structures were fixed in a 6-well plate (CELLSTAR, Greiner, Germany) using double-sided tape (Tesa, Germany). During transfer and fixation, the printed structures were always kept hydrated in a small volume of Milli-Q water, which was dispensed on top of the glass slide. After fixation, each well was filled up with Milli-Q water and nanoindentation measurements were conducted using a Pavone Nanoindenter (Optics11Life, the Netherlands) with a spherical probe (radius: 3 µm, spring constant: 0.02 N m^{-1}, Optics11Life, the Netherlands). Samples were measured at room temperature, with an approach speed of 10 µm s^{-1}. Young's moduli were determined by fitting the force–indentation curves obtained to the Hertz model in Eq. (2), where F is the applied force, E the Young's modulus, ν the Poisson's ratio, R the tip radius, and δ the indentation depth. The indentation depth was set to 300 nm, and the contact point was defined at 20% of the maximum measured force. Poisson's ratio of 0.5 was assumed. Data analysis was performed using the software DataViewer (V 2.5.7, Optics11Life, the Netherlands). For each sample, 10 individual pillar structures were measured.

$$F(\delta) = \frac{4}{3}\frac{E}{(1-\nu^2)}\sqrt{R}\delta^{\frac{3}{2}} \quad (2)$$

Transparent 3D MEA fabrication

ITO feedlines and electrodes were photopatterned on a quartz substrate (thickness: 0.5 mm) via maskless photolithography (MLA150, Heidelberg

Instruments, Germany). For high quality and easy liftoff, a double layer of photoresist consisting of LOR3B (MicroChemicals GmbH, Germany) and nlof2020 (MicroChemicals GmbH, Germany) were employed. ITO was then sputtered (nominal thickness: 250 nm, Nordiko 2000, NORDIKO Ltd., UK) and lifted off in dimethyl sulfoxide (DMSO, MicroChemicals GmbH, Germany) for 24 h at room temperature, followed by successive rinsing in acetone and IPA. The wafer was afterwards annealed in a furnace for 4 h at 400 °C. The devices were passivated with a stack of silicon oxide and silicon nitrate (nominal thickness: 800 nm) deposited *via* plasma enhanced chemical vapor deposition (SI 500 D ICPECVD System, SENTECH Instruments GmbH, Germany), followed by a thin layer of tantalum pentoxide (nominal thickness: 40 nm) deposited *via* atomic layer deposition (FlexAl ALD, Oxford Instruments, UK). The contact pads as well as the electrode openings (diameter: 24 µm) were patterned using 5.5 µm-thick etch mask based on AZ4562 resist (MicroChemicals GmbH, Germany). The passivation layer was then dry etched *via* inductively coupled plasma reactive ion etching (Oxford PL 100, Oxford Instruments, UK). The remaining photoresist was stripped in acetone and IPA. Finally, the wafer underwent saw dicing to obtain precisely cut single devices (nominal dimension: 24.22 mm × 24.22 mm). Single MEAs were washed and treated as explained above. A long working distance 20× air objective was used to print 50 µm × 50 µm × 20 µm structures on the microelectrode's openings.

Electrical measurements of 2PP printed microstructures

I-V scans were conducted on parallelepiped structures with dimensions of 150 µm × 30 µm × 40 µm, fabricated using TPL with printing parameters mentioned above. After development, structures were kept and measured in Milli-Q water. Electrical contact was established using two tungsten needles (PicoProbe, GBB Industries Inc., USA) with 2 µm diameter tips, connected to a probe station (PM5, Cascade Microtech, USA), on the very end of the structures, keeping distance between the tips fixed. The scans were performed over a voltage range from -1 V to 1 V, with a resolution of 0.1 V and a sensitivity of 100 pA.

Electrochemical impedance spectroscopy was carried out on cubical structures (50 µm × 50 µm × 20 µm), printed with a 20× air objective, connecting the contact pads of the 3D transparent MEA to the working electrode of a potentiostat/galvanostat (VSP-300, Biologic, Germany), a Pt wire as counter electrode and an Ag/AgCl pellet as reference electrode. The sinusoidal input signal was set to 10 mV by scanning a range of frequencies from 300 Hz to 1 MHz. A glass ring was glued to the substrate and filled with DPBS.

Cell interfacing

For the cell interfacing experiments, circular glass coverslips (thickness: 0.13 mm - 0.16 mm, diameter: 13 mm) were used as the base substrates. These coverslips were first cleaned and silanized following the procedure previously described. Once prepared, stylized neuron-shaped CH structures (height: 10 µm) were printed onto the functionalized glass surfaces with a 25× oil objective. Before proceeding to cell culture, all substrates used for cell culture underwent a sterilization process. First, each sample was immersed in 70% abs. ethanol (TH. Geyer, Germany) in double distilled water for 10 min, this was followed by three sequential rinses with sterile double-distilled water, where each rinse consisted of a 5-minute immersion to thoroughly remove residual ethanol. After the ethanol rinsing, the samples were submerged in fresh sterile double-distilled water and exposed to UV-C light for a minimum of 1 h. Once sterilized, the substrates were incubated with 500 µL of a poly-L-lysine (PLL) solution (Sigma-Aldrich Chemie GmbH, Germany) for 45 min at room temperature. Following incubation, excess PLL was removed by rinsing the substrates three times with sterile double-distilled water. Finally, the PLL-coated substrates were immersed in complete cell culture medium and incubated for 24 h prior to seeding.

Stability test

Stylized neuron structures were printed as mentioned in Sample preparation and sterilized with ethanol. Samples were then incubated at 37 °C in DPBS, and imaged with EVOS M5000 (Thermo Fisher Scientific Inc. Inc., Germany) monitoring possible changes in the structures or detachments over a period of 14 days ($N = 3$).

Primary neuron culture

Primary cortical neurons were isolated from embryonic day 18 Wistar rat embryos (Javier, France). The use of primary tissues in this work was approved by the state animal ethics committee, the Landesumweltamt für Natur, Umwelt und Verbraucherschutz Nordrhein-Westfalen, Recklinghausen, Germany, under permit number 81-02.04.2023.A172. The experiments were conducted in accordance with local animal protection regulations. Cortices were digested in cold 0.05% Trypsin-EDTA (Thermo Fisher Scientific Inc., Germany) for 10 min at 37 °C followed by mechanical trituration[51] and plated on substrates at a density of 100,000 cells mL^{-1} in a 24-well plate. Three to four hours after cell seeding, the medium was replaced completely with fresh B27 Plus Neuronal Culture System consisting of Neurobasal Plus medium (Thermo Fisher Scientific Inc., Germany) and B27 Plus supplement (Thermo Fisher Scientific Inc., Germany). The culturing medium was supplemented with 1% B27 Plus and 50 µg mL^{-1} gentamycin (Sigma-Aldrich Chemie GmbH, Germany).

HT22 cell culture

Mouse hippocampal neuron derived cell line HT22 (gifted from Velia Siciliano's lab, IIT, Naples, Italy) were cultured in Dulbecco's Modified Eagle Medium/Nutrient Mixture F-12 with GlutaMAX 1:1 (Thermo Fisher Scientific Inc., Germany) supplemented with 10% fetal bovine serum (Thermo Fisher Scientific Inc., Germany), 1% penicillin-streptomycin (Thermo Fisher Scientific Inc., Germany). As 80% confluence was reached, cells were detached from the culture flask and collected after 5 min of incubation in 0.05% Trypsin-EDTA. Warm media was added to quench the action of trypsin and cells were centrifuged at 700 rpm for 5 min. The supernatant was removed, and cells were resuspended in 6 mL of warm supplemented media and then counted with Trypan Blue Stain (Sigma-Aldrich Chemie GmbH, Germany) in a Countess 3 cell counter (Thermo Fisher Scientific Inc., Germany). HT-22 cells (passage 3 to passage 12) were then plated on substrates at a density of 4000 cells mL^{-1} in a 24-well plate.

Biocompatibility assay

After four days in vitro, cells were incubated for 10 min at 37 °C, 5% CO_2 with a cell medium solution (1 mL) containing ethidium homodimer (EtHD, Sigma-Aldrich Chemie GmbH, Germany) 1 µg mL^{-1}, Calcein acetoxymethyl ester (Calcein-AM, Thermo Fisher Scientific Inc., Germany) 1 µg mL^{-1} and Hoechst-33342 (Thermo Fisher Scientific Inc., Germany) 0.1 µg mL^{-1}. After incubation samples were washed once with DPBS for HT22 or Hank's Balanced Salt Solution (HBSS, Sigma-Aldrich Chemie GmbH, Germany) for pRCN and transferred into a 3 cm petri dish filled with 3 mL warm DPBS for HT22 or HBSS for pRCN, and imaged in fluorescence with EVOS M5000 (Thermo Fisher Scientific Inc., Germany) microscope equipped with 20× air objective. Five frames were obtained for each sample with randomly chosen regions of interest. Image-J software was used to quantify the number of dead and live cells, and the percentage ratio of live cells was calculated employing the following Eq. (3):

$$live\ dead\ ratio(\%) = \frac{live\ cells}{(live\ cells + dead\ cells)} * 100 \quad (3)$$

Scanning electron microscopy of primary neurons cultured on 2PP printed microstructures

Scanning electron micrographs (Gemini 1550 instrument, Leo/Zeiss, Germany) were acquired after chemical fixation and dehydration of the structures. Initially, samples were fixed with 4% paraformaldehyde (PFA, Thermo Fisher Scientific Inc., Germany) in cytoskeleton-stabilizing buffer (PEM), composed of 80 mM 1,4-piperazinediethanesulfonic acid (PIPES, Sigma-Aldrich Chemie GmbH, Germany), 5 mM ethylene glycol tetraacetic

acid (EGTA, Sigma-Aldrich Chemie GmbH, Germany), 2 mM $MgCl_2$ (Sigma-Aldrich Chemie GmbH, Germany) at pH 6.8, for 10 min at room temperature, followed by three washes in DPBS (5 min each). A secondary fixation was performed using 2.5% glutaraldehyde (GA, Sigma-Aldrich Chemie GmbH, Germany) in 0.1 M cacodylate buffer (Electron Microscopy Sciences, USA) for 2 h. Dehydration was carried out through a gradual abs. ethanol exchange, with 10 min immersions in solutions of increasing concentration (30%, 50%, 70%, 80%, 90%, and 100%) in Milli-Q water. The samples then underwent critical point drying (CPD 030, BAL-TEC Company). The CPD chamber was initially filled with 100% ethanol, into which the samples were placed. The temperature was reduced to 10 °C, and ethanol was gradually replaced with liquid CO_2 through multiple exchange cycles until the chamber was fully saturated with CO_2. The temperature was then raised to 42 °C and the pressure increased to 75 bar to reach the critical point. Finally, the chamber was depressurized, allowing the samples to dry completely. Dried specimens were mounted on SEM stubs using double-sided carbon tape and sputter coated (2 cycles, 15 mA, 0.01 mBar, 90 s, thickness: ~ 11 nm, Emitech). with a thin layer of iridium. Imaging was performed using a scanning electron microscope at an accelerating voltage ranging from 3 kV to 10 kV and working distance of 1 mm to 5 mm.

Statistical analysis

For biocompatibility analysis, three parallel cultures were prepared for each condition, and every experiment was repeated three times ($n = 3, N = 3$). For experiments involving pRCN, embryos for each individual experiment were sourced from a single mother. Each experiment used a different mother, such that two experiments did not share embryos from the same individual. The statistical analysis was performed using Python's library statmodels[52]. For the viability assay, a one-way ANOVA test followed by a Tukey's multiple comparisons test was performed to assess any effect of the substrates used on the percentage of live cells compared to PLL coated glass.

Data availability

The data that support the findings of this study are available from the corresponding author upon request.

Received: 31 July 2025; Accepted: 6 January 2026;
Published online: 30 January 2026

References

1. Rivnay, J., Wang, H., Fenno, L., Deisseroth, K. & Malliaras, G. G. Next-generation probes, particles, and proteins for neural interfacing. *Sci. Adv.* **3**, e1601649 (2017).
2. Cox-Pridmore, D. M., Castro, F. A., Silva, S. R. P., Camelliti, P. & Zhao, Y. Emerging Bioelectronic Strategies for Cardiovascular Tissue Engineering and Implantation. *Small* **18**, 2105281 (2022).
3. Procès, A., Luciano, M., Kalukula, Y., Ris, L. & Gabriele, S. Multiscale Mechanobiology in Brain Physiology and Diseases. *Front. Cell Dev. Biol.* **10**, 823857 (2022).
4. Sunwoo, S.-H., Ha, K.-H., Lee, S., Lu, N. & Kim, D.-H. Wearable and Implantable Soft Bioelectronics: Device Designs and Material Strategies. *Annu. Rev. Chem. Biomol. Eng.* **12**, 359–391 (2021).
5. Guo, B., Glavas, L. & Albertsson, A.-C. Biodegradable and electrically conducting polymers for biomedical applications. *Prog. Polym. Sci.* **38**, 1263–1286 (2013).
6. Axpe, E., Orive, G., Franze, K. & Appel, E. A. Towards brain-tissue-like biomaterials. *Nat. Commun.* **11**, 3423 (2020).
7. Yuk, H., Lu, B. & Zhao, X. Hydrogel bioelectronics. *Chem. Soc. Rev.* **48**, 1642–1667 (2019).
8. Mariano, A., Bovio, C. L., Criscuolo, V. & Santoro, F. Bioinspired micro- and nano-structured neural interfaces. *Nanotechnology* **33**, 492501 (2022).
9. Aboal-Castro, L. et al. Laser-Assisted Micropatterned 3D Printed Scaffolds with Customizable Surface Topography and Porosity for Modulation of Cell Function. *Adv. Healthc. Mater.* **14**, 2403992 (2025).
10. Sharaf, A., Frimat, J.-P. & Accardo, A. Mechanical confinement matters: Unveiling the effect of two-photon polymerized 2.5D and 3D microarchitectures on neuronal YAP expression and neurite outgrowth. *Mater. Today Bio* **29**, 101325 (2024).
11. Flamourakis, G. et al. Deciphering the Influence of Effective Shear Modulus on Neuronal Network Directionality and Growth Cones' Morphology via Laser-Assisted 3D-Printed Nanostructured Arrays. *Adv. Funct. Mater.* **35**, 2409451 (2025).
12. Pennacchio, F. A. et al. Three-dimensionally Patterned Scaffolds Modulate the Biointerface at the Nanoscale. *Nano Lett.* **19**, 5118–5123 (2019).
13. Sands, I. et al. Interface-Mediated Neurogenic Signaling: The Impact of Surface Geometry and Chemistry on Neural Cell Behavior for Regenerative and Brain-Machine Interfacing Applications. *Adv. Mater.* **36**, 2401750 (2024).
14. Jiang, Y. et al. The Roles of Micro- and Nanoscale Materials in Cell-Engineering Systems. *Adv. Mater.* **36**, 2410908 (2024).
15. Yin, J. et al. Leveraging biomimetic materials for bioelectronics. *Matter* **8**, 101961 (2025).
16. Santoro, F., Schnitker, J., Panaitov, G. & Offenhäusser, A. On Chip Guidance and Recording of Cardiomyocytes with 3D Mushroom-Shaped Electrodes. *Nano Lett.* **13**, 5379–5384 (2013).
17. Santoro, F., van de Burgt, Y., Keene, S. T., Cui, B. & Salleo, A. Enhanced Cell–Chip Coupling by Rapid Femtosecond Laser Patterning of Soft PEDOT:PSS Biointerfaces. *ACS Appl. Mater. Interfaces* **9**, 39116–39121 (2017).
18. Cho, Y. H., Park, Y., Kim, S. & Park, J. 3D Electrodes for Bioelectronics. *Adv. Mater.* **33**, 2005805 (2021).
19. Ruggiero, A. et al. Two-photon polymerization lithography enabling the fabrication of PEDOT:PSS 3D structures for bioelectronic applications. *Chem. Commun.* **58**, 9790–9793 (2022).
20. Wang, P. et al. Direct-Print 3D Electrodes for Large-Scale, High-Density, and Customizable Neural Interfaces. *Adv. Sci.* **12**, 2408602 (2025).
21. Kurselis, K., Kiyan, R., Bagratashvili, V. N., Popov, V. K. & Chichkov, B. N. 3D fabrication of all-polymer conductive microstructures by two photon polymerization. *Opt. Express, OE* **21**, 31029–31035 (2013).
22. Bansal, M. et al. Patternable Gelatin Methacrylate/PEDOT/Polystyrene Sulfonate Microelectrode Coatings for Neuronal Recording. *ACS Biomater. Sci. Eng.* **8**, 3933–3943 (2022).
23. Zhou, X., Liu, X. & Gu, Z. Photoresist Development for 3D Printing of Conductive Microstructures via Two-Photon Polymerization. *Adv. Mater.* **36**, 2409326 (2024).
24. Zhou, X. et al. Photoinduced double hydrogen-atom transfer for polymerization and 3D printing of conductive polymer. *Nat. Synth.* **3**, 1145–1157 (2024).
25. Sanjuan-Alberte, P. et al. Development of Conductive Gelatine-Methacrylate Inks for Two-Photon Polymerisation. *Polymers* **13**, 1038 (2021).
26. Restaino, M. et al. In Situ Direct Laser Writing of 3D Graphene-Laden Microstructures. *Adv. Mater. Technol.* **6**, 2100222 (2021).
27. Dadras-Toussi, O. et al. Multiphoton Lithography of Organic Semiconductor Devices for 3D Printing of Flexible Electronic Circuits, Biosensors, and Bioelectronics. *Adv. Mater.* **34**, 2200512 (2022).
28. Lichade, K. M., Shiravi, S., Finan, J. D. & Pan, Y. Direct printing of conductive hydrogels using two-photon polymerization. *Addit. Manuf.* **84**, 104123 (2024).
29. Amruth, C., Singh, A. K., Sharma, A., Corzo, D. & Baran, D. Micro-3D Printed Conductive Polymer Composite via Two-Photon Polymerization for Sensing Applications. *Adv. Mater. Technol.* **9**, 2400290 (2024).
30. Blasco, E. et al. Fabrication of Conductive 3D Gold-Containing Microstructures via Direct Laser Writing. *Adv. Mater.* **28**, 3592–3595 (2016).
31. Tanaka, T., Ishikawa, A. & Kawata, S. Two-photon-induced reduction of metal ions for fabricating three-dimensional electrically conductive metallic microstructure. *Appl. Phys. Lett.* **88**, 081107 (2006).

32. Vyatskikh, A. et al. Additive manufacturing of 3D nano-architected metals. *Nat. Commun.* **9**, 593 (2018).
33. Wang, F. et al. 3D Printed Implantable Hydrogel Bioelectronics for Electrophysiological Monitoring and Electrical Modulation. *Adv. Funct. Mater.* **34**, 2314471 (2024).
34. Zhao, G. Z. et al. Feng. Rational design of electrically conductive biomaterials toward excitable tissues regeneration. *Prog. Polym. Sci.* **131**, 101573–101573 (2022).
35. Tropp, J. et al. Conducting Polymer Nanoparticles with Intrinsic Aqueous Dispersibility for Conductive Hydrogels. *Adv. Mater.* **36**, 2306691 (2024).
36. Rivnay, J. et al. Structural control of mixed ionic and electronic transport in conducting polymers. *Nat. Commun.* **7**, 11287 (2016).
37. Li, H. et al. PEDOTs-Based Conductive Hydrogels: Design, Fabrications, and Applications. *Adv. Mater.* **37**, 2415151 (2025).
38. Pennacchio, F. A. et al. Three-Dimensional Microstructured Azobenzene-Containing Gelatin as a Photoactuable Cell Confining System. *ACS Appl. Mater. Interfaces* **10**, 91–97 (2018).
39. Yue, K. et al. Synthesis, properties, and biomedical applications of gelatin methacryloyl (GelMA) hydrogels. *Biomaterials* **73**, 254–271 (2015).
40. Van Den Bulcke, A. I. et al. Structural and Rheological Properties of Methacrylamide Modified Gelatin Hydrogels. *Biomacromolecules* **1**, 31–38 (2000).
41. Brigo, L. et al. 3D high-resolution two-photon crosslinked hydrogel structures for biological studies. *Acta Biomater.* **55**, 373–384 (2017).
42. Spencer, A. R. et al. Electroconductive Gelatin Methacryloyl-PEDOT:PSS Composite Hydrogels: Design, Synthesis, and Properties. *ACS Biomater. Sci. Eng.* **4**, 1558–1567 (2018).
43. Testore, D., Zoso, A., Kortaberria, G., Sangermano, M. & Chiono, V. Electroconductive Photo-Curable PEGDA-Gelatin/PEDOT:PSS Hydrogels for Prospective Cardiac Tissue Engineering Application. *Front Bioeng. Biotechnol.* **10**, 897575 (2022).
44. Chou, C.-C. et al. Injectable GelMA–PEDOT:PSS conductive hydrogel for cardiac-tissue engineering and integrated organic electrochemical transistor–based bioelectronic patch for biosensing and controlled extracellular vesicle release. *Chem. Eng. J.* **523**, 168573 (2025).
45. Furlani, F. et al. Electroconductive and injectable hydrogels based on gelatin and PEDOT:PSS for a minimally invasive approach in nervous tissue regeneration. *Biomater. Sci.* **10**, 2040–2053 (2022).
46. Lopez-Larrea, N. et al. Fast Visible-Light 3D Printing of Conductive PEDOT:PSS Hydrogels. *Macromol. Rapid Commun.* **45**, 2300229 (2024).
47. Wloka, T., Gottschaldt, M. & Schubert, U. S. From Light to Structure: Photo Initiators for Radical Two-Photon Polymerization. *Chem. – A Eur. J.* **28**, e202104191 (2022).
48. Tarricone, G., Carmagnola, I. & Chiono, V. Tissue-Engineered Models of the Human Brain: State-of-the-Art Analysis and Challenges. *J. Funct. Biomater.* **13**, 146 (2022).
49. Paleti, S. H. K. et al. Impact of doping on the mechanical properties of conjugated polymers. *Chem. Soc. Rev.* **53**, 1702–1729 (2024).
50. Claaßen, C. et al. Quantification of Substitution of Gelatin Methacryloyl: Best Practice and Current Pitfalls. *Biomacromolecules* **19**, 42–52 (2018).
51. Brewer, G. J., Torricelli, J. R., Evege, E. K. & Price, P. J. Optimized survival of hippocampal neurons in B27-supplemented neurobasal™, a new serum-free medium combination. *J. Neurosci. Res.* **35**, 567–576 (1993).
52. Seabold, S. & Perktold, J. Statsmodels: Econometric and Statistical Modeling with Python. *Scipy* https://doi.org/10.25080/Majora-92bf1922-011 (2010).

Acknowledgements

The authors thank the Helmholtz Nano Facility (HNF) at Forschungszentrum Jülich and the Central Laboratory for Micro- and Nanotechnology (ZMNT) at RWTH Aachen for facilitating the microfabrication of the transparent MEA, with the support of Marko Banzet (Forschungszentrum Jülich) and Jochen Heiß (Institute of Materials in Electrical Engineering 1, RWTH Aachen). The authors thank Elmar Neumann (Forschungszentrum Jülich) for supporting in SEM sample preparation and imaging. The authors thank Dr. Velia Siciliano, PI of SynBioLab@IIT, Naples (IT) for gifting HT22 cells. The authors thank Christoph Räuber for supporting in NMR spectra acquisition. The authors thank Alma Fernandez Naumann for the original illustrations of this manuscript, generated with BioRender and Inkscape. The authors thank Erik Noetzel-Reiss and Yannik Herfs (IBI-2, Forschungszentrum Jülich) for supporting the 3D microstructures visualization with IMARIS software. The authors thank Frank Josten from Carl Zeiss Microscopy Deutschland GmbH for giving the possibility to use Apotome 3. F.S. thanks the European Research Council starting Grant BRAIN-ACT No. 949478. M.B., F.S. and L.D.L. thank the DFG ME3T grant GRK 2415. S.I. and A.O. thank the DFG InnoRetVision grant GRK 2610.

Author contributions

V.C. and F.S. developed the initial idea and led the experimental design and the writing of this manuscript. M.B. contributed to the design, fabrication, characterization and data analysis of the presented work. M.G. carried out the fabrication of ITO-based MEAs. T.C.S. assisted the mechanical characterization and data interpretation. N.S. supported cell culture experiments. S.I. contributed infrastructure and experimental implementation for the clean room fabrication. L.D.L. contributed to the experimental implementation. A.O. contributed to infrastructure and experimental implementation. All authors contributed to the data analysis and manuscript writing.

Funding

Open Access funding enabled and organized by Projekt DEAL.

Competing interests

The authors declare no competing interests.

Additional information

Supplementary information The online version contains supplementary material available at https://doi.org/10.1038/s41528-026-00529-5.

Correspondence and requests for materials should be addressed to Valeria Criscuolo.